ANALYSIS OF SEISMIC SPECTRAL ATTENUATION BASED ON WIGNER-VILLE DISTRIBUTION FOR SANDSTONE RESERVOIR CHARACTERIZATION - A CASE STUDY FROM THE WEST SICHUAN DEPRESSION, CHINA

XIOYANG WU and TIANYOU LIU

Institute of Geophysics and Geomatics, China University of Geosciences, Wuhan, Hubei 430074, P.R.China

ABSTRACT

Wu, X. and Liu, T., 2010. Analysis of seismic spectral attenuation based on Wigner-Ville distribution for sandstone reservoir characterization - a case study from the West Sichuan depression, China. *Journal of Seismic Exploration*, 19: 69-85.

       A mass of previous work has shown the application of seismic spectral decomposition for low frequency shadows detection and stratigraphic mapping. In this paper, we further analyze the characteristics of spectral attenuation in fractured sandstone reservoirs saturated with different fluids by Wigner-Ville distribution (WVD) based method. We give a description on the geometric structure of cross-terms due to bilinear nature of WVD with a multicomponent signal composed of three Gaussian time-frequency atoms. Then cross-terms are eliminated using improved WVD with time and frequency independent Gaussian kernels as smoothing windows, what is called the smoothed pseudo WVD (SPWVD). At last the SPWVD is applied to spectral decomposition of seismic data from West Sichuan depression of China. We focus our study on the comparison of characteristics of spectral attenuation in order to verify whether SPWVD can differentiate different fluids content. It shows that prolific gas reservoirs show higher peak spectral amplitude at higher peak frequency, which attenuate faster than low quality gas reservoirs and dry or wet reservoirs. SPWVD is able to separate prolific gas reservoirs from low-quality gas reservoirs and dry or wet reservoirs. This can be regarded as a spectral attenuation signature for future exploration in the study area.

KEYWORDS: Wigner-Ville distribution, Gaussian kernel function, spectral attenuation, fluids, fractured sandstone reservoir.

INTRODUCTION

Recently, there has been an uplift of interest in spectral decomposition for seismic interpretation since Partyka et al. (1999) provide a novel means of utilizing it for highlighting channels over large 3D seismic surveys. A first class of spectral decomposition is given by atomic decomposition, such as the short-time Fourier transform (STFT) and wavelet based approaches, which decompose non-stationary signals as the linear combination of time-frequency atoms. Over the past ten years, atomic spectral decomposition has been widely studied as direct hydrocarbon indicator (DHI, Castagna et al., 2003; Sinha et al., 2005; Goloshubin et al., 2006; Wang, 2007; Li and Zheng, 2008; Wu and Liu, 2009) because of its ability to significantly enhance the exhibition of low frequency shadows (Taner et al., 1979) related to hydrocarbon reservoir.

An alternative class of spectral decomposition is the energy distribution. This set of methods distributes energy of signals over time-frequency plane. The representative Wigner-Ville distribution (WVD) has a better resolution amongst all time-frequency representations of this class as WVD values are determined by all the values rather than a part of the analyzed signal limited by a time window. However, WVD being bilinear in nature introduces cross-terms for a multicomponent signal. Cross-terms have significant amplitudes interference and make WVD not so widely used in the processing of seismic data. Boudreaux-Bartels and Wiseman (1987) once employ auto and cross WVD analysis to separate different wave components of the multicomponent borehole seismic signals. Moriya and Niitsuma (1996) use Choi-Williams distribution (Choi and Williams, 1989) with exponential function as kernel for precise determination of P-wave arrival times. Recently, WVD based methods are applied to seismic spectral decomposition for reservoir characterization. A comparison between STFT and continuous wavelet transform (CWT) and the WVD based method (Rauch-Davies and Ralston, 2005; Ralston et al., 2007) shows that the WVD based method is of superior resolutions for seismic field data. A spectral analysis of Rick wavelets model by Li and Zheng (2008) also illustrate higher resolutions of WVD based method.

Much work has been conducted on spectral decomposition for low frequency shadows detection. But mechanism of such effects is still poorly understood. As has been pointed out by Ebrom (2004), seismic processing can also bring low frequency shadows to seismic profiles. Some basic research and laboratory experiments have been done in order to confirm the relationship between reservoirs and low frequency shadows. Goloshubin, et al. (2002) and Korneev, et al. (2004) conduct Laboratory ultra-sonic experiments to investigate the differences of reflections from dry-water and oil-saturated layers and observe that the low frequency "bright spot" with phase shift is associated with oil saturation. They try to explain this phenomenon using a "frictional-viscous" model. Silin et al. (2004) create an asymptotic representation of seismic

reflection in low-frequency domain from a fluid-saturated porous medium. Chapman et al. (2005) and Liu et al. (2006) insist that the existence of high attenuation and related dispersion in hydrocarbon saturated zones is a strong candidate mechanism for the frequency anomalies. Chen et al. (2008) study spectral decomposition of far-angle stack seismic images and show that reservoir fluid type is a main factor controlling spectral response. As less research is carried out on analysis of spectral attenuation characteristics of different fluid saturated reservoirs, in this paper, after giving a description on the theoretical framework of WVD and the suppression of cross-terms, we apply the improved WVD method to spectral decomposition of seismic data from the West Sichuan depression of China for fractured tight sandstone gas reservoir characterization. We analyze the distinction between different frequency-dependent spectral amplitude sections. As different fluid saturated reservoirs may attenuate seismic reflection energy of different frequency components, it is possible for high-resolution spectral decomposition approach to detect this phenomenon. We further compare the characteristics of spectral attenuation of different fluids encountered by nine wells.

GEOMETRIC STRUCTURE OF CROSS-TERMS

The WVD of signal x (t) is defined in time domain as

$$W(t,f) = \int_{-\infty}^{\infty} x(t + \tau/2)x^*(t - \tau/2)e^{-j2\pi f\tau}d\tau \ , \tag{1}$$

where τ is the time delay variable, $x^*(t)$ means the complex conjugate of $x(t)$. Eq. (1) shows that WVD is regarded as Fourier transform for t of $x(t+\tau/2)x^*$ (t-t/2), which is the instantaneous autocorrelation function of $x(t)$. WVD preserves time and frequency shifting invariance and satisfies the marginal properties (Cohen, 1995). Nevertheless, owing to the bilinear nature of WVD, the spectrum of a multicomponent signal will have cross-terms between each pair of the signal components. Cross-terms have no physical means and hamper interpretation. In practice, the analyzed signal needs to be sampled at least twice of the Nyquist sampling rate for alias-free purpose when using Fourier transform, as any particular frequency value of the product $x(t+\tau/2)x^*(t-\tau/2)$ occurs at twice of $x(t)$. Furthermore, analytic signal is required as to real signal, since the spectrum of analytic signal has nonezero values only for positive frequencies. For a seismic signal s(t), we use the complex trace (Taner et al., 1979).

$$S(t) = s(t) + jH[s(t)] \ . \tag{2}$$

H[s(t)] is the Hilbert transform of s(t) as the imaginary part of S(t).

Consider a multicomponent synthetic signal (Fig. 1) consisting of three Gaussian time-frequency atoms (real Morlet wavelet). Each atom is expressed as the following format,

$$s(t) = e^{-(\alpha/2)(t-t_0)^2} \cos\omega_0 t \ , \tag{3}$$

where (t_0, ω_0) is the time-frequency locations with (0.3 s, 35 Hz), (0.9 s, 35 Hz), (0.9 s, 15 Hz) for each atom. The sampling space is 10 milliseconds.
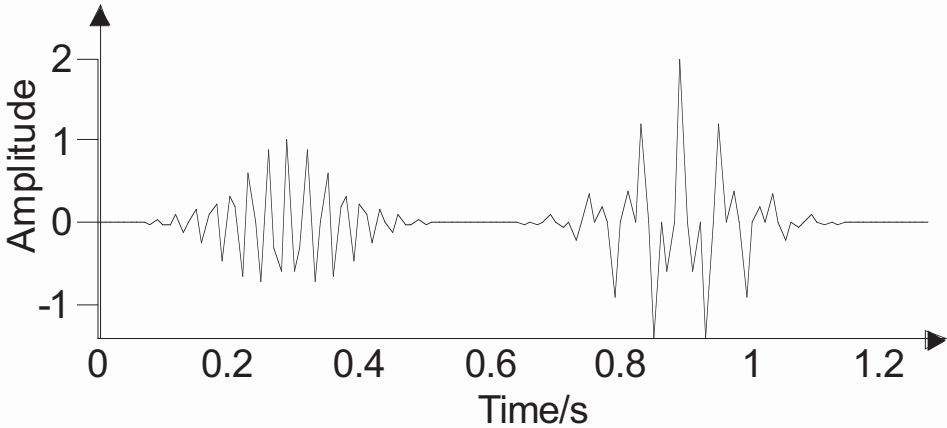

Fig. 1. A synthetic real signal consisting of three Gaussian time-frequency atoms with a sampling space of 10 milliseconds.

Fig. 2 displays the WVD spectrum for the synthetic signal. We find there is serious cross-terms interference due to the bilinear property of WVD. Furthermore, the characteristic of spectral symmetry for a real signal, namely $WVD_x(t,f) = WVD_x(t, -f)$, has lead to spectral redundancy and appearance of cross-terms near zero frequency area.

In order to reduce the interference of cross-terms, we substitute with the complex Gaussian atoms (complex Morlet wavelet) which is the analytic signal of s(t) expressed as

$$s(t) = e^{-(\alpha/2)(t-t)^2}(\cos\omega_0 t + i\sin\omega_0 t) \ , \tag{4}$$

Fig. 3 is the WVD spectrum of the analytical signal. Note that there is no cross-terms near zero frequency zone and the three Gaussian atoms are well located in the time-frequency plane. However, high-amplitude cross-terms oscillating along time and frequency axis still exist at the center of every two atoms.
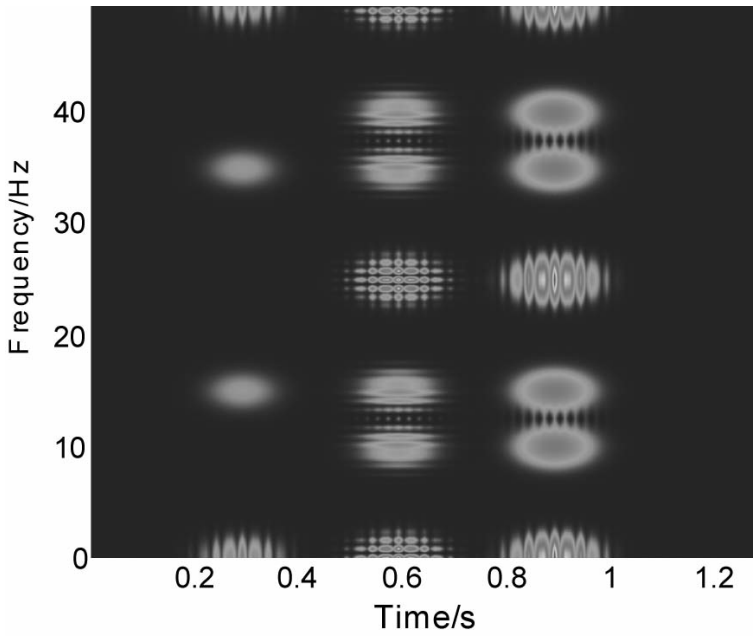
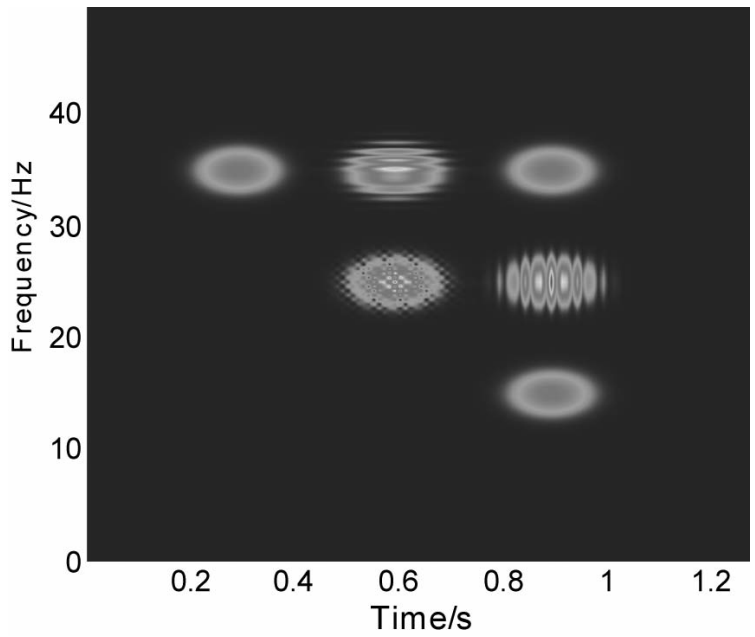Fig. 2. The WVD spectrum of the synthetic signal.

Fig. 3. The WVD spectrum of the analytical signal of the synthetic signal.

ELIMINATING CROSS-TERMS WITH SMOOTHING WINDOWS

The definition of WVD requires a knowledge of $x(t + \tau/2)x^*(t - t/2)$ from $\tau = -\infty$ to $\tau = +\infty$. In other words, the value of WVD is determined by all the values of x(t). For convenient computation purpose, we often replace the infinite integrals in equation (1) by finite integrals with a window function of time length T sliding along the time axis. Thus, the WVD of a windowed signal is called pseudo-WVD (PWVD), defined as

$$PW(t,f) = \int_{-\infty}^{\infty} h(\tau)x(t + \tau/2)x^*(t - \tau/2)e^{-j2\pi f\tau}d\tau \quad . \tag{5}$$

The function h(t) is defined in the time interval of $[-T/2, T/2]$. Windowing operation is equivalent to a frequency smoothing of WVD. Fig.4 shows the PWVD spectrum of the analytical signal [using a 310 ms Gaussian window for h(t)]. It exhibits that the oscillation along frequency axis in Fig. 3 is smoothed away. But the oscillation along time axis still exists between the following two atoms: (0.9 s, 35 Hz), (0.9 s, 15 Hz).
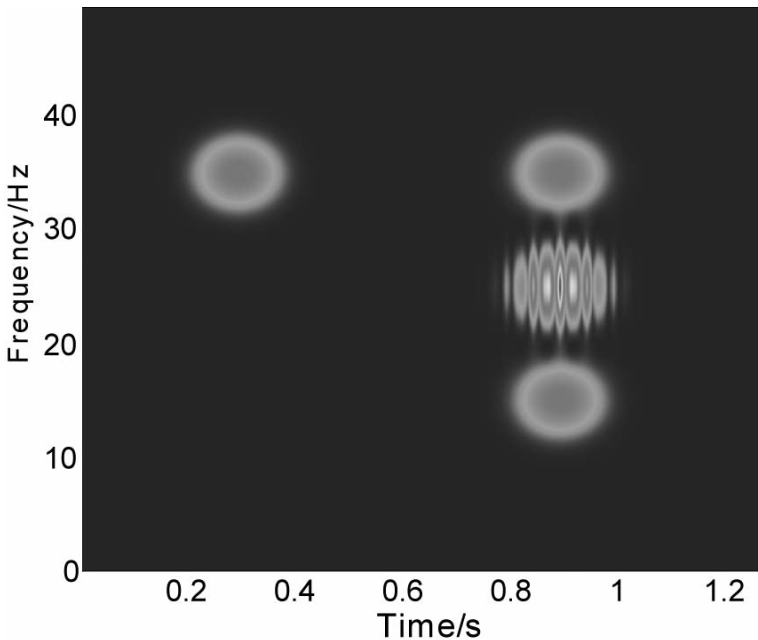

Fig. 4. The pseudo WVD spectrum of the analytical signal. Note that cross-terms oscillating along frequency axis in Fig. 3 are suppressed. However, cross-terms oscillating along the time axis still exist.

To further smooth away the cross-terms oscillating along the time axis, another window is added to eq. (5) as

$$SPW(t,f) = \int_{-\infty}^{\infty} h(\tau) \int_{-\infty}^{\infty} g(t - \eta)x(\eta + \tau/2)x^*(\eta - \tau/2)d\eta e^{-j2\pi f\tau}d\tau , \quad (6)$$

where g(t) is the time smoothing window. This is known as smoothed pseudo WVD (Claasen and Mecklenbrauker, 1980; Novak and Novak, 1993). When the two smoothing windows h(t) and g(t) are both Gaussian function, i.e.,

$$\phi(t,\omega) = g(\omega)h(t) = e^{-\alpha t^2 - \beta\omega^2} , \quad \alpha \geq 0, \ \beta \geq 0, \quad (7)$$

where α and β are used to modulate the bandwidth of the Gaussian function, SPWVD can be continuous transformed from spectrogram (SPEC, square of STFT) to WVD. WVD provides superior time - frequency resolution and more serious cross-terms, while SPEC takes on almost no cross-terms but inferior time − frequency resolution. SPWVD allows optimal trade-off between the two extremes if α and β are selected appropriately.

Fig. 5 is the spectrum calculated by SPWVD with a 410 ms Gaussian window for h(τ) and 810 ms for g(t). There shows little cross-terms but appears a loss in time-frequency resolution. From Figs. 3, 4 and 5, it is found that the smoothing windows in time and frequency domain have lead to an increase of bandwidth of auto-terms. However, it is possible to reach an optimal time and frequency resolution by properly choosing α, β and the window length.

APPLICATION FOR SANDSTONE GAS RESERVOIR CHARACTERIZATION

The study area is located in West Sichuan Province of China, of which the reservoir is a type of fractured super-tight sandstones in the second member of the XuJiahe formation of the upper Triassic (Tx2), buried at a depth of about 5000 m. Exploration practice of this area shows that the gas reservoirs are of low porosity and permeability but with super high pressure (Tang et al., 2008). Fig.6 displays the Time depth of T51 corresponding to the top of Tx2 and the locations of nine wells. RMS amplitude slice between T51 and T511 (the bottom of Tx2) was calculated to analyze the sedimentary facies. As shown in Fig. 7, there mainly exist two facies belts: braid river sedimentary facies and lake sedimentary facies. The lake sedimentary facies belts consist of shales and the braid river sedimentary facies belts are composed of deep dense sandstones. We can see the northeastward paleo-rivers dramatically in Fig. 7. The width of this type of rivers varies from 100 to 180 m, buried at a depth of about 5000 m.
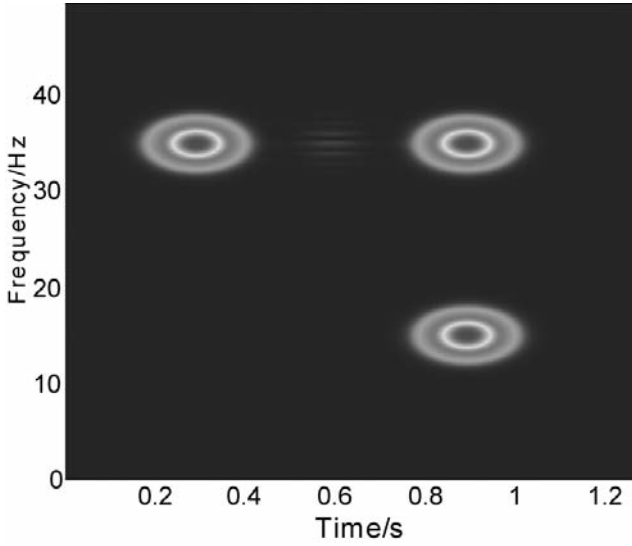
Fig. 5. The smoothed pseudo WVD spectrum of the analytic signal. Cross-terms have been suppressed significantly although the bandwidth of auto-terms is increased.
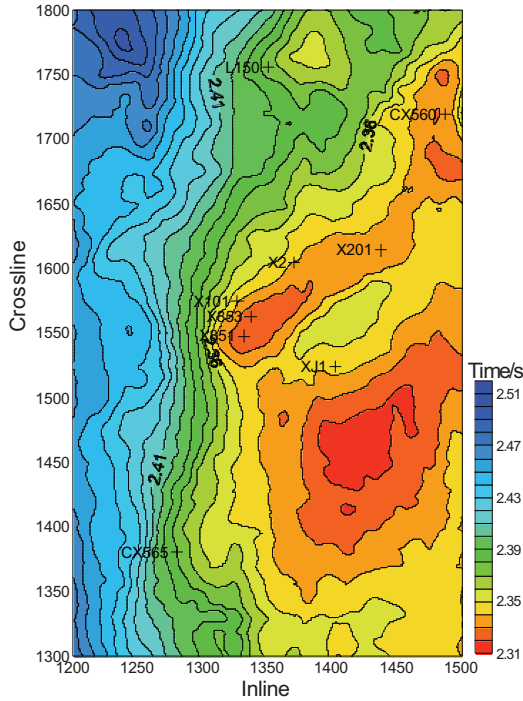

Fig. 6. Time depth of T51 corresponding to the top of the second member of XuJiahe formation, which reflects the paleogeomorphology in the upper Triassic period.
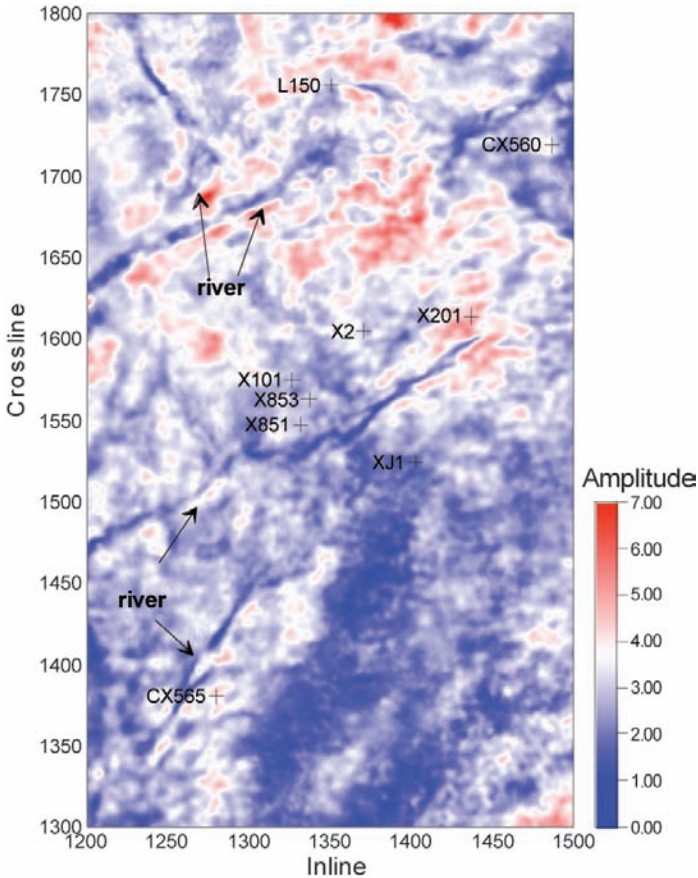
Fig. 7. RMS amplitude slice between T51 and T511. Low values correspond to lake sedimentary facies and high values correspond to braid river sedimentary facies.

Fig. 8 displays a 2D seismic connect - well line extracted from the 3D data set. The sampling space is 2 ms and the trace space is 20 m. A long time of deep burial in the Indosinian and Yanshanian periods has made the sandstones of high density (2.5-2.7 g/cm^3) and low acoustic interval transit time (50-65 μs/m). X851 is the first well aimed at this type of deep tight sandstone reservoirs with an accidental high average output of about 150×10^4 m^3/d. It indicates that the deep Xujiahe formation possesses large exploration potential. However, subsequently, the dry well L150 and the wet well CX565 with gas output less than 0.1×10^4 m^3/d shows that the gas deposits are not large-area distributed. Traditional methods such as STFT, routine seismic attribute, coherence, impedance inversion which are effective for detecting shallow gas reservoirs cannot reach the required resolutions. Spectral decomposition via SPWVD was performed on this 2D seismic section.
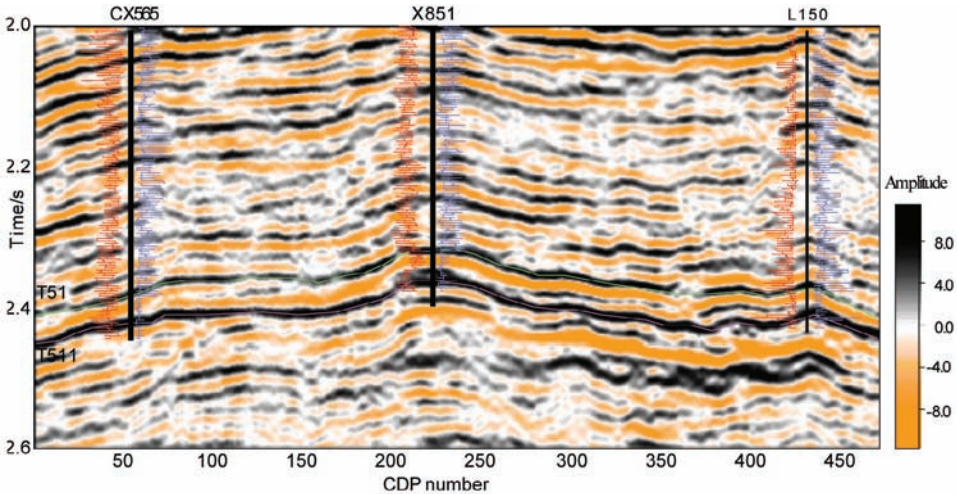
Fig. 8. Stack section across the three wells CX565, X851 and L150 from 3D seismic data with density well-log (drawn with red color) on the left and acoustic well-log (drawn with blue color) on the right. The target reservoir is between horizon T51 and T511.

A set of different isofrequency sections is shown in Fig. 9. For X851 at the section of 20 Hz, there is slight high energy cluster at the position of reservoir. This energy cluster becomes stronger at 40 Hz and 60 Hz and appears as frequency shadow, but gradually attenuates at 80 Hz and 100 Hz. For CX565 and L150, the energy clusters appear at the section of 40 Hz rather than 20 Hz, moreover, it only lasts to the section of 60 Hz. For more clarity purpose, we calculate the instantaneous spectral amplitude (ISA). Fig. 10 displays the frequency gathers of average ISA between T51 and T511. It is found that the values of high spectral amplitudes at X851 are greater than that of CX565 and L150. It has a wider energy cluster lasting from 20 to 100 Hz. Notice that the highest spectral amplitudes occurred at CDP 250-350. There is still energy cluster at the 100 Hz section in Fig. 9 (e). It is possibly due to impedance difference between shales and super-tight sandstone with no fractures. As we know that impedance difference caused by lithologies change can have significant influence on seismic events than reservoirs saturated with fluids.
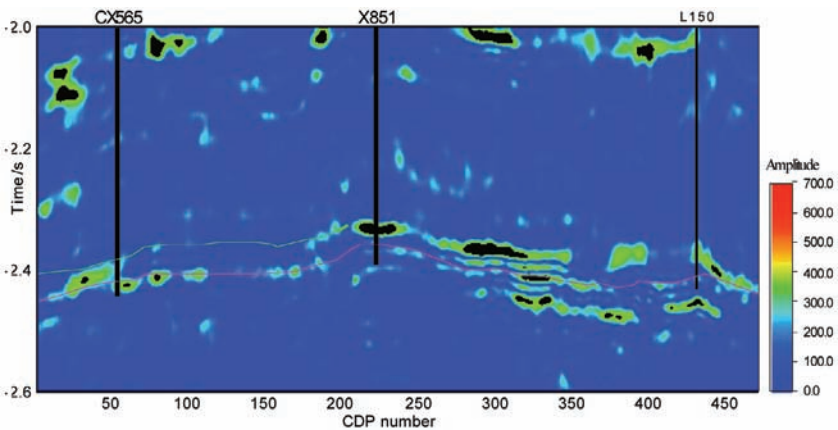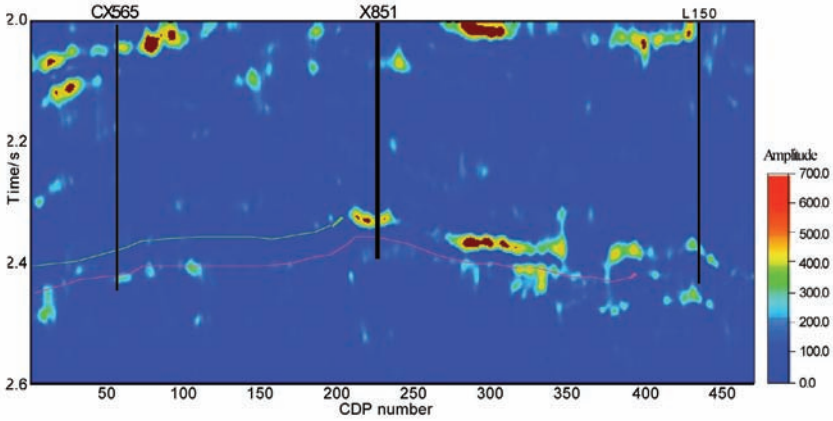
(a) 20 Hz
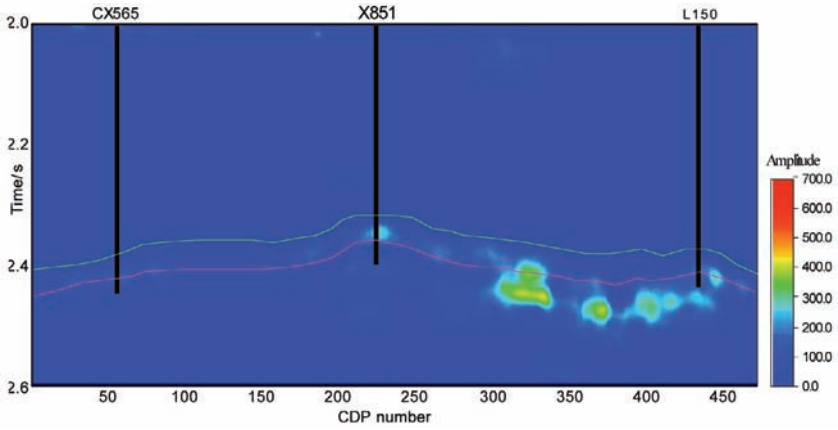
(b) 40 Hz
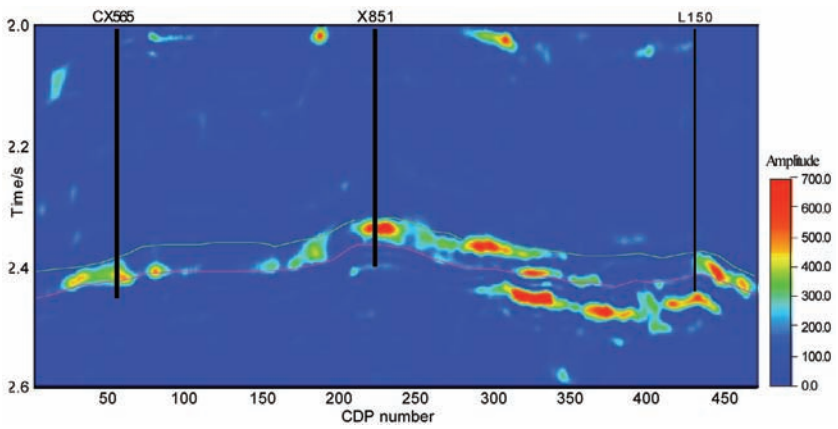
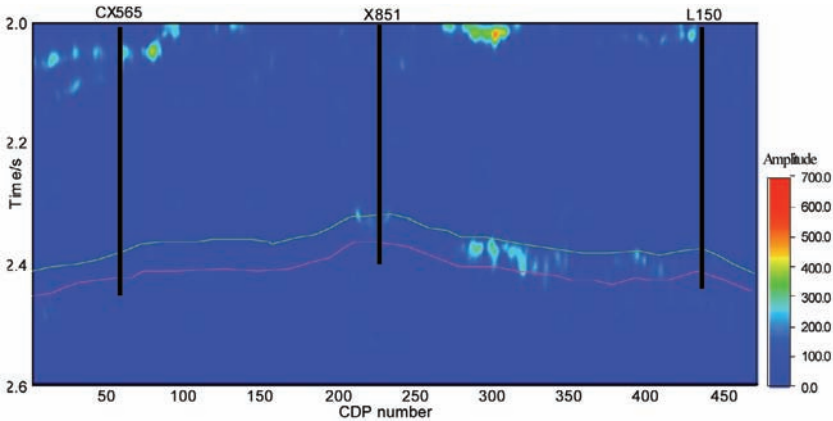(c) 60 Hz

(d) 80 Hz

(e) 100 Hz

Fig. 9. A set of isofrequency sections at 20 Hz, 40 Hz, 60 Hz, 80 Hz and 100 Hz for the seismic section in Fig. 8 with SPWVD.

Fig. 11 shows the frequency-average ISA curves between T51 and T511 at the CDP numbers corresponding to locations of the nine wells. X2 and X201 are prolific gas wells with an output more than 50×10^4 m^3/d. X853 is a relative low-yield well. CX560, XJ1 and X101 are wet wells. Table 1 displays four attribute parameters of the frequency- average ISA curves in Fig. 11. Bandwidth is defined as the frequency interval of spectral amplitude bigger than $0.707 \times$ Peak amplitude. The attenuation gradient is calculated as the negative slope between the amplitude interval of $(0.85-0.55) \times$ Peak amplitude with the peak frequency as initial frequency.
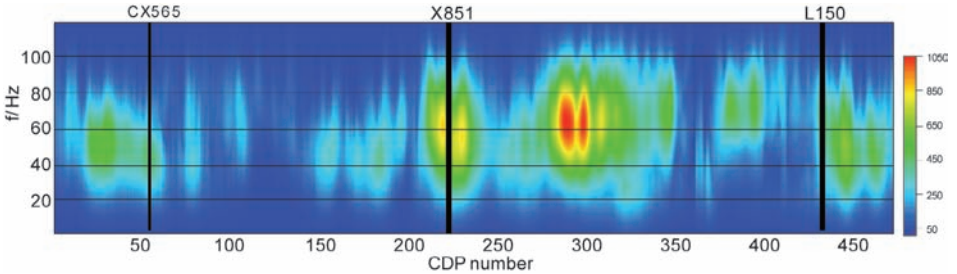
Fig. 10. Frequency gathers of average ISA between T51 and T511, black lines indicates the location of wells. X-axis represents the CDP direction and y-axis is the frequencies ranging from 2 - 120 Hz.

Fig. 11 and Table 1 indicate that the prolific gas wells have bigger peak amplitude upwards of 600 than the dry well and wet wells. Furthermore, the curves of X851, X2 and X853 illustrate that the more gas saturated in reservoir, the higher peak amplitude would be. It is inferred that the super high-pressure gas deposits saturated in the reservoir not only gives rise to low frequency shadows but also has an influence on the impedance which affect the spectral amplitudes to a certain extent. Table 1 also shows that the peak frequencies of gas saturated reservoirs are over 50 Hz, but of the dry or wet wells are lower under 50 Hz. And it is found from the values of attenuation gradient that spectral amplitudes of x851, X2 and X201 attenuate faster than X853 and the dry or wet wells. The characteristics above indicate that SPWVD is able to separate prolific gas reservoirs from low-quality gas reservoirs and dry or wet reservoirs. However, the similarity of spectral amplitude between X853 and CX560 indicates that there seems to be little obvious difference between low-quality gas reservoirs and dry or wet reservoirs. In fact, X853 is a low-yield well with an output of 7×10^4 m^3/d, which gives rise to little increase on the peak amplitude (from 397.5 to 452.5) and the attenuation gradient (from 8 to 10).

To delineate the spatial distribution of the gas reservoir, we calculate the average ISA slices between T51 and T511 from 3D seismic volume with SPWVD. Fig. 12 (a) displays the spectral amplitude slice at 40 Hz. Note that the gas reservoir area around X851 is only about 0.2 km^2. The fluid content of reservoir changes fast from high quality gas saturated at X851 to low quality at X853, then with water saturated at X101. X201 and X2 are also located at positions of high energy cluster which last to the slice of 80 Hz with some attenuation. As shown in Fig. 12, we divide the spectral amplitude into three classes.
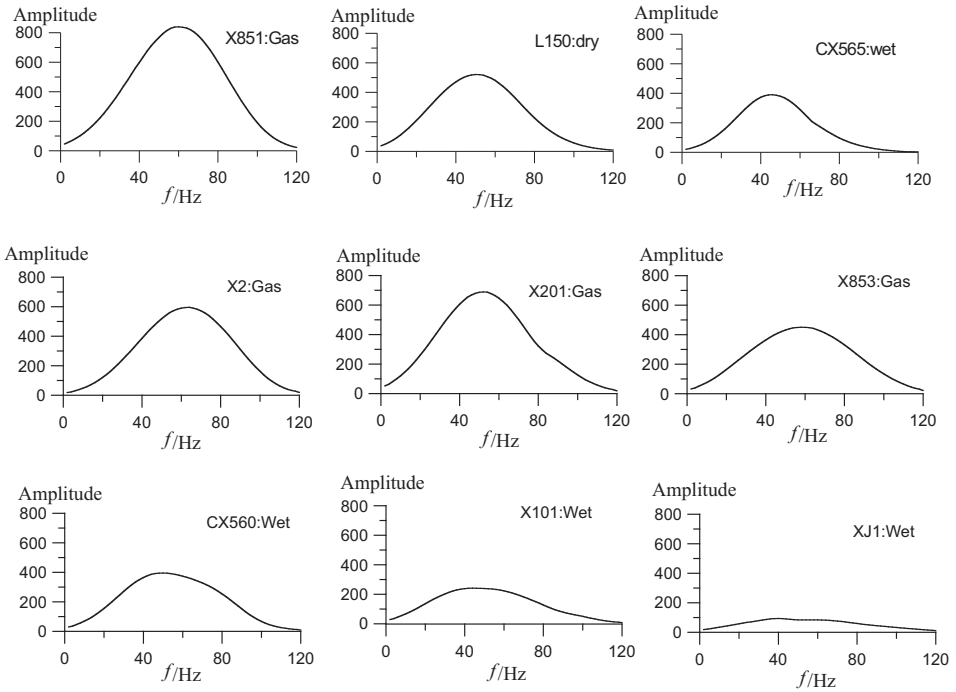
Fig. 11. Frequency-average ISA curves of the nine wells between T51 and T511.

Table 1. Attribute parameters of the nine Frequency- average ISA curves in Fig. 11.

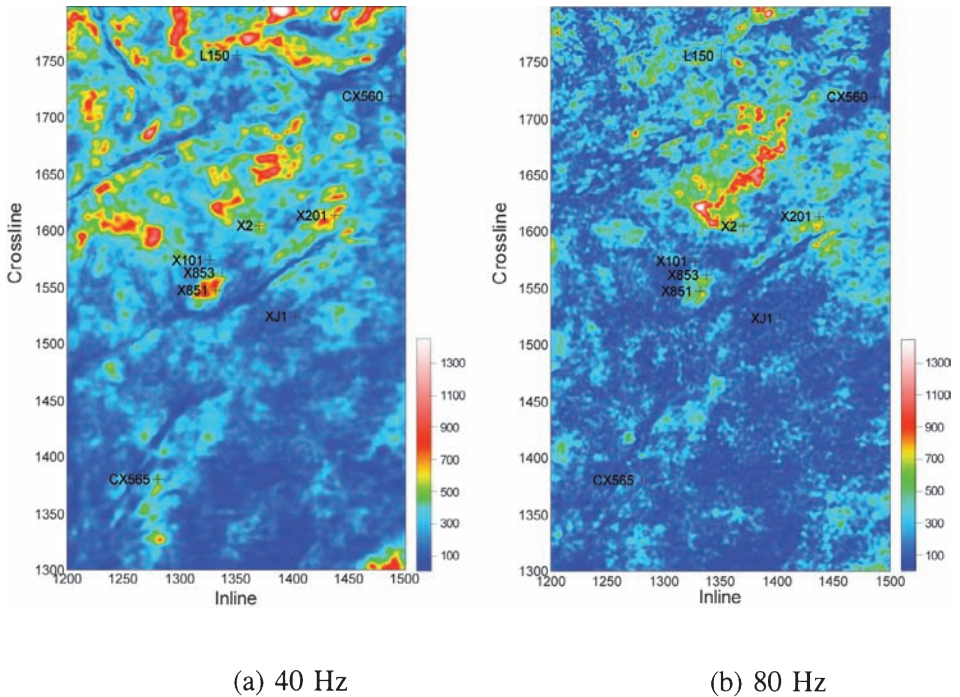| Well ID	X851	X853	X2	X201	L150	CX560	CX565	X101	XJ1
Fluid types	prolific gas	gas	prolific gas	prolific gas	dry	wet	wet	wet	wet
Peak amplitude	840.4	452.5	597.9	694.3	521	397.5	390.1	242.9	95.8
Peak frequency(Hz)	60	60	62	52	50	50	46	42	40
Bandwidth(Hz)	44	48	42	40	40	48	32	48	52
Attenuation gradient	21.8	10.0	15.2	18.1	13.5	8.0	13.2	5.3	1.6

(a) 40 Hz   (b) 80 Hz

Fig. 12 Average ISA slices between T51 and T511 at 40 Hz and 80 Hz by SPWVD.

(a) The first class: high amplitudes at low frequencies and low amplitudes at high frequencies. Attribute to that attenuation is strongly affected by the porous-medium properties and fluid saturation (Hauge, 1981; Sams et al., 1997; Goloshubin and Korneev, 2000), reservoirs may located at where there are high amplitudes at low frequencies and low amplitudes at high frequencies, furthermore, higher amplitudes at low frequencies imply prolific gas deposits, while not so high amplitudes may related to low-quality gas or wet zones.

(b) The second class: High amplitudes in almost all bandwidth. This class is possibly due to high impedance difference between shales and super tight sandstones with no fractures, such as the area up of X2 (including CDP 250-350 in Fig. 10) in Fig. 12.

(c) The third class: Low amplitudes in almost all bandwidth. This class is related to shales belong to lake sedimentary facies.

CONCLUSIONS

We have given a detailed description on using Gaussian kernel functions to smooth away cross-terms interference caused by the bilinear nature of WVD. In our opinion, the SPWVD is of higher "cost-performance" in resolution and computational time than STFT and matching pursuit. Furthermore, SPWVD is not just a mathematical method. It has an explicit physical sense, which represents the energy density distribution on time-frequency plane. The case study of super-tight sandstone reservoirs indicates that not only spectral decomposition with SPWVD can be used to detect low frequency shadows, but also it has the potential to separate prolific gas reservoirs from low-quality gas reservoirs and dry or wet reservoirs. Prolific gas reservoirs show higher peak spectral amplitude at higher peak frequency, which attenuate faster than low quality gas reservoirs and dry or wet reservoirs. This can be regarded as a spectral attenuation signature for further exploration in the study area.

ACKNOWLEDGMENTS

REFERENCES

Boudreaux-Bartels, G. and Wiseman, P., 1987. Wigner distribution analysis of acoustic well logs. Acoust., Speech, and Signal Proces., IEEE Internat. Conf. on ICASSP '87, 12: 2237- 2240.

Castagna, J.P., Sun, S. and Siegfried, R.W., 2003. Instantaneous spectral analysis: Detection of low-frequency shadows associated with hydrocarbons. The Leading Edge, 22: 120-127.

Chapman, M., Liu, E. and Li, X-Y, 2005. The influence of abnormally high reservoir attenuation on the AVO signature. The Leading Edge, 24: 1121-1125.

Chen, G., (**ALL NAMES**), 2008. Spectral-decomposition to reservoir fluids from a deepwater West Africa reservoir. Geophysics, 73: 23-30.

Choi, H.I. and Williams, W.J., 1989. Improved time frequency representation of multicomponent signals using the exponential kernels. IEEE Transac. Signal Proces., 37: 862-871.

Claasen, T. and Mecklenbrauker, W., 1980. The Wigner distribution: a tool for time-frequency signal analysis. Philips J. Res., 35: 217-250.

Cohen, L., 1995.Time-frequency analysis. Prentice Hall Inc., New York.

Ebrom, D., 2004. The low frequency gas shadows in seismic sections. The Leading Edge, 23: 772.

Goloshubin, G.M. and Korneev, V.A., 2000. Seismic low frequency effects for fluid saturated porous media. Expanded Abstr., 70th Ann. Internat. SEG Mtg., Calgary, Alberta: 976-979.

Goloshubin, G.M., Korneev, V.A. and Vingalov, V.M., 2002. Seismic low-frequency effects from oil-saturated reservoir zones. Expanded Abstr., 72nd Ann. Internat. SEG Mtg., Salt Lake City: 1813-1817.

Goloshubin, G.M., (**ALL NAMES**), 2006. Reservoir imaging using low frequencies of seismic reflections. The Leading Edge, 25: 527-531.

Hauge, P.S., 1981. Measurements of attenuation from vertical seismic profiles. Geophysics, 46: 1548-1558.

Korneev, V.A., (**ALL NAMES**), 2004. Seismic low frequency effects in monitoring fluid-saturated reservoirs. Geophysics, 69: 522-532.

Li, Y. and Zheng, X., 2008. Spectral decomposition using Wigner-Ville distribution with applications to carbonate reservoir characterization. The Leading Edge, 28: 1050-1057.

Liu, E., (**ALL NAMES**), 2006. Applications of spectral decomposition for AVO analyses in the west of Shetland. Expanded Abstr., 76th Ann. Internat. SEG Mtg., New Orleans: 279-282.

Moriya, H. and Niitsuma, H., 1996. Precise detection of a P-wave in low S/N signal by using time-frequency representations of a triaxial hologram. Geophysics, 61: 1453-1466.

Novak, P. and Novak, V., 1993. Time/frequency mapping of the heart rate, blood pressure and respiratory signals. Med. Biol. Eng. Comput. 31: 103-110.

Partyka, G., Gridley, J. and Lopez, J., 1999. Interpretational applications of spectral decomposition in reservoir characterization. The Leading Edge, 18: 353-360.

Rauch-Davies, M. and Ralston, M., 2005. Spectral decomposition - transform methods and fluid and reservoir prediction case study. 67th EAGE Conf., Madrid.

Ralston, M., (**ALL NAMES**), 2007. General method to reduce crossterm interference in the Wigner-Ville decomposition. Expanded Abstr., 77th Ann. Internat. SEG Mtg., San Antonio: 870-874.

Sams, M.S., Neep, J.P., Worthington, M.H. and King, M.S., 1997. The measurement of velocity dispersion and frequency-dependent intrinsic attenuation in sedimentary rocks. Geophysics, 62: 1456-1464.

Silin, D.B., (**ALL NAMES**), 2004. A hydrologic view on Biot's theory of poroelasticity. Lawrence Berkeley National Lab. Paper-54459, Univ. of California.

Sinha, S.P., (**ALL NAMES**), 2005. Spectral decomposition of seismic data with continuous-wavelet transform. Geophysics, 70: 19-25.

Taner, T.H., Koehler, F. and Sheriff, R.E., 1979. Complex seismic trace analysis. Geophysics, 44: 1041-1063.

Tang, J., Zhang, S. and Li, X.-Y., 2008. PP and PS seismic response from fractured tight gas reservoirs: a case study. J. Geophys. Engin., 5: 92-102.

Wang, Y., 2007. Seismic time-frequency spectral decomposition by matching pursuit. Geophysics, 72: 13-20.

Wu, X. and Liu, T., 2009. Spectral decomposition of seismic data with reassigned smoothed pseudo Wigner-Ville distribution. J. Appl. Geophys., 68: 386-393.